NANO LETTERS

Letter

pubs.acs.org/NanoLett

Role of Defects in Ion Transport in Block Copolymer Electrolytes

Yu Kambe,[†,‡] Christopher G. Arges,[§] David A. Czaplewski,[∥] Moshe Dolejsi,[†,‡] Satya Krishnan,[†] Mark P. Stoykovich,[†] Juan de Pablo,[†,‡] and Paul F. Nealey*[,†,‡]

[†]Pritzker School of Molecular Engineering, University of Chicago, 5640 S. Ellis Avenue, Chicago, Illinois 60637, United States

[‡]Institute for Molecular Engineering, Materials Science Division, Argonne National Laboratory, 9700 S. Cass Avenue, Lemont, Illinois 60439, United States

[§]Cain Department of Chemical Engineering, Louisiana State University, Baton Rouge, Louisiana 70803, United States

[∥]Center for Nanoscale Materials, Argonne National Laboratory, 9700 S. Cass Avenue, Lemont, Illinois 60439, United States

S *Supporting Information*

ABSTRACT: Ion conducting block copolymers can overcome traditional limitations of homopolymer electrolytes by phase separating into nanoarchitectures that can be simultaneously optimized for two or more orthogonal material properties such as high ion conductivity and mechanical stability. A key challenge in understanding ion transport properties of these materials is the difficulty of extracting structure−function relationships without having complete knowledge of all nanoscale transport pathways in bulk samples. Here we demonstrate a method for deriving structure-transport relationships for ion conducting block copolymers using thin films and interdigitated electrodes. Well-defined and directly imaged structure in films of poly(styrene)-*block*-poly(2-vinylpyridine) is controlled using techniques of directed self-assembly then the poly(2-vinylpyridine) is selectively converted into an ion conductor. The ion conductivity is found to be directly proportional to the total number of connected paths between electrodes and the path length. A single defect such as a dislocation anywhere in the path of an ion conducting route disconnects and precludes that pathway from contributing to the conductivity and results in an increase in the dielectric parameter of the film. When all the ion conduction pathways are blocked between electrodes, the conductivity is negligible, 4 orders of magnitude lower compared to a completely connected morphology and the dielectric parameter increases by a factor of 50. These results have profound implications for the interpretation, design, and processing of block copolymer electrolytes for applications as ion conducting membranes.

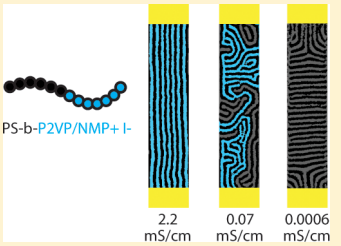

KEYWORDS: *Block copolymer electrolytes, thin film, ion transport, directed assembly*

Ion conducting polymer membranes play a central role in the development of safer and more efficient electrochemical devices such as fuel cells,[1] electrolyzers,[2] and redox flow batteries.[3−8] Membranes composed of a single component often suffer from trade-offs between high ionic conductivity and mechanical robustness.[9] Block copolymer electrolytes (BCEs) are promising candidates as membrane materials because of the opportunity to simultaneously optimize two (or more) orthogonal properties.[10,11] The two components of a diblock BCE, for example, can be optimized for both ion conductivity and mechanical properties. The blocks can then self-assemble into a structure of nanoscale ion conducting channels that are periodically distributed among mechanically rigid but ion insulating domains. Morphologies commonly formed by BCEs include gyroid networks,[12] lamellae,[13] and hexagonally packed cylinders,[14] ostensibly offering transport in three, two, and one dimensions, respectively.

Structure−property relationships in BCEs are challenging to derive because the periodic domain structure of BCEs formed through self-assembly are well-ordered only locally at the submicron scale but transport properties are typically measured over macroscopic dimensions, on the scale of tens to thousands of microns. At this device scale, the materials can be described as consisting of multiple grains. The implications of this structure are that, regardless of the local BCE morphology, the materials have the potential to conduct in three dimensions, the conduction pathways are likely to be tortuous, and mechanisms of transport across grain boundaries and defects must be considered. Effective medium theory (EMT)[15] is a methodology to characterize the dependence of ion transport on morphology and is written in its simplest form as

$$\sigma_{BCE} = f\phi_{COND}\sigma_{HOMO} \quad (1)$$

where σ_{BCE} is the conductivity of the BCE, σ_{HOMO} is the conductivity of the homopolymer that is chemically identical to the conducting block of the BCE, ϕ_{COND} is the volume fraction of the conducting block, and f is a tortuosity factor. The anticipated value of f for each grain in a BCP morphology is uncomplicated: f equals one for gyroids and for sphere-forming BCPs with majority phase conducting in all directions,

Received: April 29, 2019
Revised: June 19, 2019
Published: June 24, 2019

DOI: 10.1021/acs.nanolett.9b01758
Nano Lett. XXXX, XXX, XXX−XXX

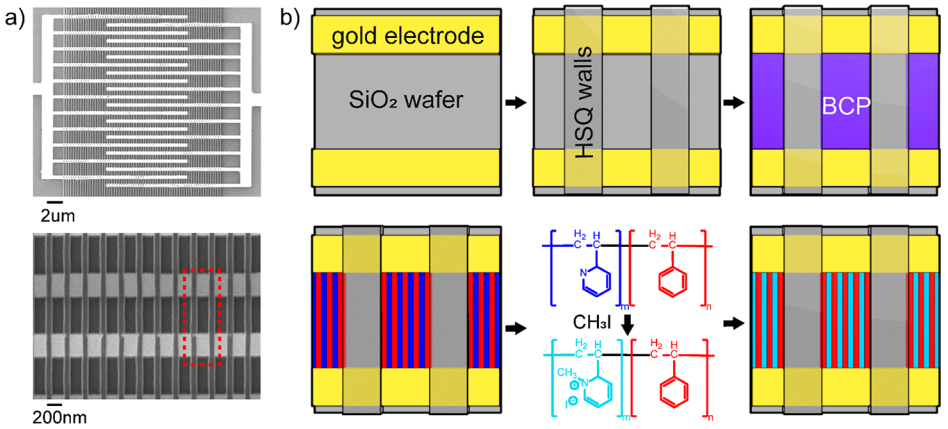

Figure 1. Schematic and results showing the fabrication and assembly processes for the graphoepitaxy interdigitated electrodes and the BCE. (a) SEM micrographs of the interdigitated electrodes with the gold electrodes appearing as the bright horizontal bars and the HSQ guiding topography as vertical stripes that form 200 nm by 1 μm trenches (single trench highlighted by a red box). (b) Fabrication schematic where the device is fabricated on a 1 μm thick SiO_2 substrate (top to bottom, left to right).

while f equals one for lamellae and cylinders in the directions parallel to the domains, and zero in the transverse directions. Theoretical values of f have been determined by Sax and Ottino[15] for multigrained BCP films assuming no impediments to transport across defects and grain boundaries. They determined transport to be isotropic in the bulk, and f to be 1 for bicontinuous morphologies such as gyroids, 1 for sphere-forming BCES where the majority phase is ion conducing, 0.33 for cylinder-forming BCEs where the minority is ion conducting, and 0.66 for lamellae forming BCE, of primary interest in this work. Hallinan and Balsara[16] have reviewed the conductivities of many different bulk and multigrain BCE systems with varying morphologies and tabulated or calculated the values of f. In the review and cited literature, the values of f reported for lamellae systems range from as low as 0.01 to within error of the theoretical value of 0.66. The majority of the reported material systems exhibited conductivities of the BCE that were not consistent with an EMT description. These included high molecular weight, lamella-forming BCPs such as polystyrene-*block*-poly(ethylene oxide) (PS-*b*-PEO) that have f values as low as 0.015,[17] and lamellae forming BCEs that were aligned using external fields in an attempt to mitigate the effect of tortuosity described above that have f values below 0.1.[18] In the few studies where the reported values of f were within an order of magnitude of the values predicted for multigrained samples, (1) the materials' systems were either lamellae forming BCPs with small grain sizes at the scale of the lamellar period itself, such as PS-*b*-PEO that reach an f value of 0.2[19,20] or (2) fully microphase-separated, lamellae-forming BCPs with high volume fractions of low molecular weight ionic liquids (ILs) with f values approaching the theoretical value of 0.66.[21] As noted by many researchers, the information required to build a unifying, fundamental understanding of transport in BCE systems is a measurement of the structure-conductivity relationship under conditions in which the structure of the material is known quantitatively, especially as it relates to the role of transport across defects and grain boundaries. However, characterization of the structure at the scale of individual domains or conduction pathways, on the scale of 10−20 nm, throughout the entire volume at the device scale, for example, a membrane of 100 μm in thickness, is difficult or impossible.[22−24]

Here we report the measurement of structure−electrochemical property relationships in lamellae-forming BCEs using thin films and interdigitated electrodes. The use of thin films enables quantitative structural characterization, and the use of interdigitated electrodes results in measurements with high signal-to-noise ratios in electrochemical impedance spectroscopy. Fabrication of connected, partially connected, and unconnected morphologies between electrodes is achieved by rudimentary implementation of the techniques of directed self-assembly, and these structural motifs are analogous to grain boundary and defect structures found in the bulk. Conductivity is found to be directly proportional to the number and length of domains of the BCE that are connected from one electrode to the other. Any conducting domain within the film with even a single impeding defect (e.g., a dislocation) does not contribute to the conductivity and increases the dielectric parameter of the material. Films with no connecting pathways exhibit conductivities more than 4 orders of magnitude lower and a dielectric parameter that is an order of magnitude higher than the connected film. These results signify that defects and grain boundaries play a central role in determining the electrochemical properties of self-assembling nanostructured electrolytes and are key parameters to understand and control in the design and processing of these materials.

The schematic for the fabrication of devices is shown in Figure 1. Gold interdigitated electrodes (IDEs) were fabricated on top of a silicon wafer with a 1 μm thick thermally grown oxide. Ninety nanometers of thick gold with a 10 nm Ti adhesion layer were deposited and patterned using ebeam lithography and liftoff techniques. The resulting IDE features 1 μm wide electrode teeth that overlap counter electrodes by 20 μm with a 1 μm separation distance. The teeth are arranged in an alternating sequence with each electrode going to one of the large contact pads for a total of 40 electrode teeth per pole. Following the fabrication of the IDE, 80 nm thick hydrogen silsesquioxane (HSQ) resist was cast on top of the IDE and patterned using electron beam (ebeam) lithography. The resulting HSQ structure formed rectangular grating structures perpendicular to the electrode axis consisting of 200 nm trenches on a 400 nm pitch as shown in Figure 1a. The HSQ grating and the gold electrodes formed elevated walls creating 200 nm by 1 μm isolating trenches where the polymer could be

DOI: 10.1021/acs.nanolett.9b01758
Nano Lett. XXXX, XXX, XXX−XXX

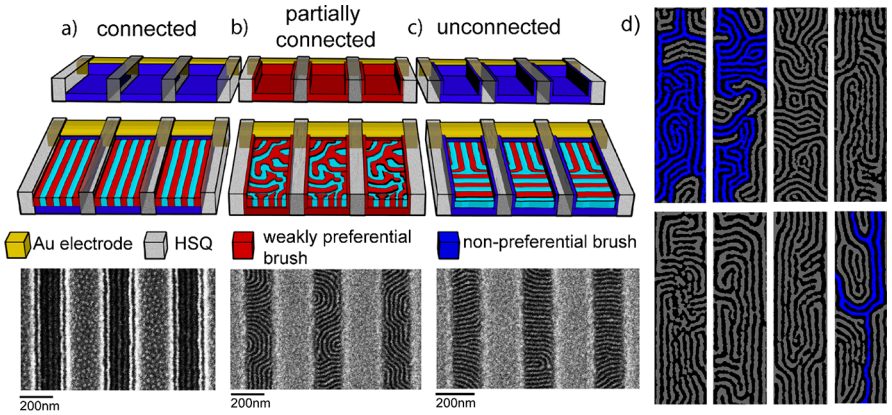

Figure 2. Orientation of the PS-*b*-P2VP domains relative to the HSQ guiding stripes and the electrodes that form the individual trenches. Schematic and SEM micrograph of (a) connected structure (b) partially connected, (c) unconnected orientation. (d) Partially connected morphology SEM micrographs after image flattening and path identification where disconnected paths are labeled gray and the connected domains are labeled blue.

confined and manipulated into different morphologies. Precisely 3950 identical trenches were fabricated on each IDE for polymer confinement.

The substrate, HSQ features, and electrodes were modified with polymer brushes at different stages during the fabrication process to induce the formation of three distinct BCE structures. Next, a film of lamellar-forming polystyrene-*block*-poly(2-vinylpyridine) (PS-*b*-P2VP) was spin coated onto the IDEs, solvent annealed in acetone, and dried such that all the polymer in the device area was confined in the trenches formed by the gold and the HSQ walls. The phase separated BCP film was then functionalized to become a BCE by exposing the film to methyl iodide (MeI) vapor for 24 h. As reported previously under these conditions, approximately 50% of the P2VP repeat units were functionalized with a fixed quaternary ammonium cation (NMP^+) and a free iodide anion (I^-). The BCE film was subsequently equilibrated in an environment with 95% relative humidity (95% RH) at 25 °C for 6 h. The volume fraction of the P2VP/NMP^+ I^- block increased from 50% to 58% after functionalization and hydration (see Supporting Information).[25] The absorbed water dissociates the iodide from the cation and plasticizes the P2VP/NMP^+I^- domain such that the Tg of the conducting blocks are below room temperature. The samples were characterized using alternating current (ac) electrochemical impedance spectroscopy (EIS) with a range of frequencies from 1 MHz to 0.1 Hz with a perturbation voltage of 10 mV.

The morphology of the BCE films after deposition, annealing, and functionalization on the device depended on the engineered boundary conditions of the trenches within the IDEs. The SiO_2 substrate, the HSQ side walls, and the gold surfaces[26] without chemical modification are all preferentially wet by one block of the BCP. PS preferentially wetted the HSQ and the gold surfaces, whereas P2VP preferentially wetted the bare SiO_2 substrate. The substrate, HSQ walls, and the gold surfaces were chemically modified at different stages of the fabrication process to be nonpreferential in wetting toward the BCP by grafting or physisorbing hydroxyl-terminated poly(styrene-*rand*-2-vinylpyridine) (P(S-*r*-2VP)-OH) brushes.[27] Under conditions in which a P(S-*r*-2VP)-OH brush was deposited onto the substrate prior to the fabrication of the HSQ guiding lines, and the monomeric mole fraction of PS in the brush was 0.685, graphoepitaxial assembly of the BCP occurred in the trenches with preferential wetting of the HSQ sidewalls, neutral (SiO_2-brush) bottom surfaces, and neutral (gold) sidewalls. With these boundary conditions, the BCP domains assembled perpendicular to the substrate and uniformly parallel to the HSQ walls with each domain forming a straight and continuous pathway between pairs of electrodes (Figure 2a). In this morphology, seven natural periodicities of PS-*b*-P2VP/NMP^+ I^- were assembled parallel to the HSQ walls. In our previous work,[25] we extracted the periodicity of the BCP to be 28 nm. Therefore, in an unconfined film the seven periods in parallel would result in a film width of 196 nm, which is consistent with the separation distance between the two HSQ walls. This morphology will be referred to as the "connected" structure. Second, samples were fabricated after depositing a different P(S-*r*-2VP)-OH brush that was weakly preferential to P2VP (monomeric mole fraction of PS in the brush equal to 0.48) on all surfaces of the devices after the HSQ fabrication. Under these conditions, the BCP domains assembled perpendicular to the substrate but in a fingerprint pattern in the plane of the film (Figure 2b). This morphology will be referred to as the "partially connected" structure. Finally, when the neutral P(S-*r*-2VP)-OH brush was deposited after the HSQ fabrication, all surfaces of the confining trenches were nonpreferential in wetting toward the copolymer. Under these boundary conditions, the BCP domains assembled perpendicular to the substrate, perpendicular to the gold electrodes, and perpendicular to the HSQ walls. Because of the aspect ratio, there was a section in the middle of the trenches over which the lamellae spanned from one HSQ wall to the other with no domains forming pathways between electrodes (see Figure 2c). This morphology will be referred to as the "unconnected" structure. Representative SEM images are shown in Figure 2d and connected domains from one electrode (top to bottom) to another in the images are identified and labeled in blue.

Two additional types of samples were prepared to compare and contrast with the results of the controlled morphologies. For the first sample, a P2VP homopolymer of comparable molecular weight to the P2VP block of the BCP (M_n = 22 000 g mol^{-1}) was deposited on the IDE with the HSQ features, annealed, and functionalized under identical protocols to the BCE. This sample will be referred as the "homopolymer" sample. For the second sample, the HSQ grating features were

DOI: 10.1021/acs.nanolett.9b01758
Nano Lett. XXXX, XXX, XXX−XXX

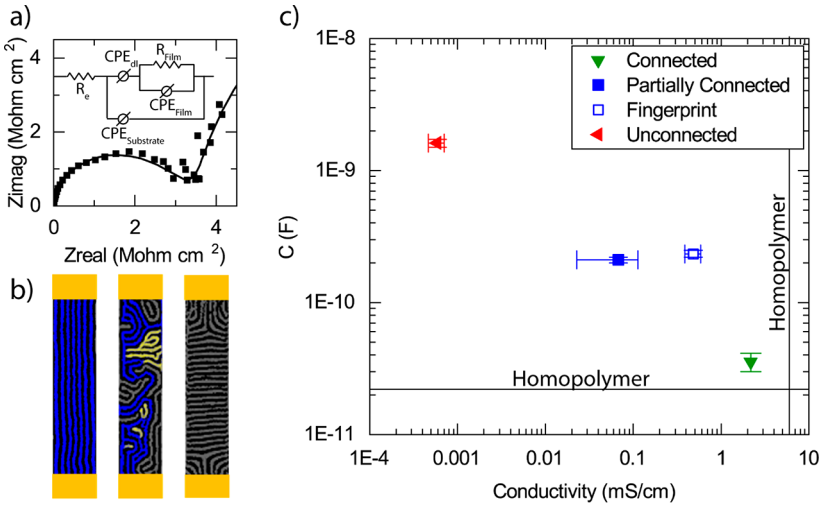

Figure 3. SEM and EIS results correlating the ion conduction pathways to electrochemical behavior. (a) Multivariable fit of EIS data for the connected structure using a custom equivalent circuit diagram to simulate the charge transport pathway. (b) Analyzed SEM micrographs of ion conduction pathways (percolated paths labeled in blue with nonparticipating sections in yellow) in segmented HSQ trenches showing (left to right) connected, partially connected (confined), and disconnected orientations. (c) Calculated C and conductivity for each structure orientation with performance limitations for the PS-*b*-P2VP/NMP$^+$ I$^-$ system (solid lines) calculated from the homopolymer impedance values.

not fabricated on top of the IDE. P(S-*r*-2VP)-OH brush was deposited over the entire surface to form a uniformly nonpreferential substrate. Then the BCP was deposited, annealed, and functionalized to form a morphology that will be referred to as the "fingerprint" structure.

An equivalent circuit model with the elements representing material and device properties to capture the essential physics of the system was used to derive the resistance and dielectric values related to the transport of ions in the polymer films from the EIS data. Recently Sharon et al.[28] reported on the conditions and system parameters for which the IDEs and circuit model yield quantitative material transport properties for ion conducting polymer films. The model is comprised only of circuit elements that have physical manifestations in the charge transport in the IDE configuration. In this study, the model consists of resistors (R) and constant phase elements (CPE) in the setup shown in Figure 3a: R_{film} and CPE_{film} capture the resistance and dielectric behavior of the polymeric material between the electrodes, respectively, CPE_{dl} models the ion depletion double-layer at the polymer−electrode interface, CPE_{SiOx} represents the dielectric behavior of the SiO_2 substrate, and $R_{electrode}$ models the electrode resistance. Conductivity (σ) of the polymer was calculated using from the value of R_{film} using the following equation

$$\sigma = \frac{d}{R_{film} L t (N-1)} \quad (2)$$

where N is the number of electrode teeth in the interdigitated array, t is the film thickness of the polymer in the trench, d is the separation distance between the edges of electrodes, and L is the length of overlap between adjacent electrodes for the polymer not including the areas occupied by the HSQ.

Capacitance (C) is derived from the CPE_{film} in the equivalent circuit model by using the following equation

$$C = \frac{(R_{film} Q^{-1})^{1/a}}{R_{film}} \quad (3)$$

where Q and a are the fitting parameters of the CPE_{film}. The unit of the Q is S*s^a. Note that CPEs are used instead of pure capacitor elements in the circuit model to improve the fit to the data. However, all values of a from modeling the EIS data were above 0.8, indicating that CPE_{film} was behaving as, and can be interpreted as, a near pure capacitor element. Figure 3a provides representative electrochemical data (scatter plot) in the form of a Nyquist plot and the fit (solid line) for the BCE with the partially connected structure. The values used for the calculation of the σ and C are tabulated in the Supporting Information.

The electrochemical behavior of BCEs in the EIS experiments showed marked differences as a function of structure. A log−log plot of the values of σ and C derived from the EIS data for the connected, disconnected, and partially connected BCE structures is shown in Figure 3c. The solid lines also shown in Figure 3c are the $\sigma_{homopolymer}$ and $C_{homopolymer}$ values for the homopolymer that correspond to the electrochemically active block of the BCEs. Several features in the log−log plot stand out. First, the σ of the homopolymer and the connected structure are relatively high, ∼2 to 6 mS/cm, and C of the homopolymer and the connected structure are relatively low, ∼3 × 10^{-11} F. For comparison, hydrated Nafion 117 has a conductivity of 79 mS/cm and C of 9 × 10^{-10} F when conditioned at 25 °C and 95% RH.[29] Second, σ_{BCE} of the unconnected structure was 4 orders of magnitude smaller than σ_{BCE} of the connected structure or σ_{HOMO}, so it was negligible in comparison. The fact that there is no conductivity when there are no domains connecting the electrodes highlights the integrity of the samples and experimental procedures. There are no unanticipated or unwanted pathways for conduction in the samples, such as through a layer of swollen polymer on the surface, through a layer of condensation of the surface, through the brush materials, or through the underlying substrate. Third, C of the unconnected structure was a factor of 50 higher than the connected structure, indicating the presence of trapped charge. Fourth, the values of the σ_{BCE} and the C of the partially connected structure were intermediate between the connected and unconnected structures, suggesting that σ_{BCE} is proportional to the number of connected domains, and that C was proportional to the number of isolated domains, dead ends, or

DOI: 10.1021/acs.nanolett.9b01758
Nano Lett. XXXX, XXX, XXX−XXX

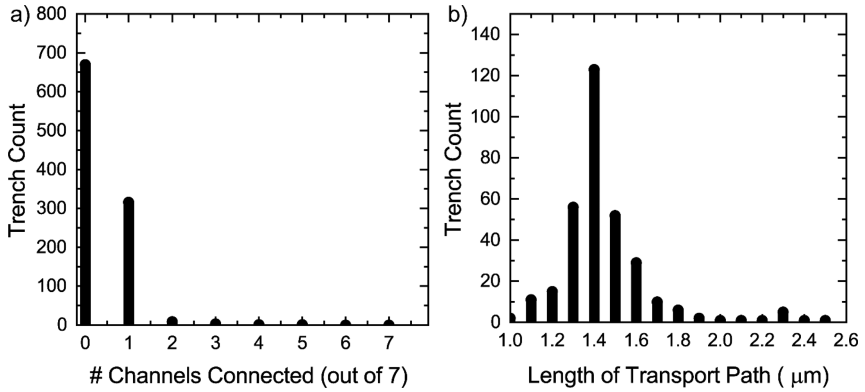

Figure 4. Extracted structure data of the partially connected morphology using visual analysis software showing (a) the total number of connected conduction paths where the total number of conduction channels is at a bottleneck, and (b) the total number of trenches as a function of the length of the conduction pathway.

ion trapping defects. Fifth, the σ_{BCE} value of the fingerprint structure was a factor of 7 larger than the partially connected film while the C stayed about the same. This suggests that there are more conduction pathways in the fingerprint structure, but there is still a significant volume of "dead" paths. The electrochemical structure−transport properties of the BCE films are discussed in quantitative fashion below.

It is important to note that the absolute conductivity and C values of the connected morphology are close but not equal to the values of the homopolymer. The ability to probe a fully connected structure allows us to decouple and independently characterize the parameters f and ϕ_{COND} in the EMT (eq 1). Using experimental values of σ_{HOMO} and σ_{BCE} equal to 6 and 2.2 mS/cm (see Supplemental Table 1), and f = 1 in eq 1, ϕ_{COND} of the connected structure is calculated to be 0.37, a value substantially lower than the estimated volume fraction of the hydrated P2VP/NMP^+ I^- in the BCE of 0.58. Unlike the P2VP/NMP^+ I^- homopolymer, the PS-*b*-P2VP/NMP^+ I^- BCE contains domain interfaces with PS over which the P2VP/NMP^+ I^- and PS are mixed over the length scale of a few nanometers.[30] P2VP/NMP^+ I^- in the interfacial regions does not likely contribute to conductivity due to the presence of even small concentrations of PS. The mechanisms by which PS may reduce the conductivity when mixed with P2VP/NMP^+ I^- include the following: (1) a reduction of local charge carrier concentration due to the hydrophobic PS lowering the local hydration levels, (2) a reduction in ionic mobility due to slower segmental dynamics of P2VP/NMP^+ I^- near the interface with glassy PS, or (3) a reduction in ion hopping probability due to the dilution of active sites by the PS. The mechanisms for reduced conductivity near the interface of conducting rubbery and nonconducting glassy domains have been reported previously for the PS-*b*-PEO system.[31,32] If we assume that all of the P2VP/NMP^+ I^- that does not contribute to conductivity resides at domain interfaces, then the width of those interfacial regimes is approximately 3 nm (see Supporting Information on calculating inactive interfacial width from conductivity), a value consistent with the width of the interface in block copolymer theory calculated using the Flory−Huggins interaction parameter χ.[30,33,34] Additionally, the value of C derived from the EIS data for the connected film (2.83 nF) is close to that of the homopolymer (2.5 nF) but slightly higher. We attribute this increased C to impeded transport of ions near domain interfaces where the P2VP/NMP^+ I^- is nonconductive.

A comparison between defect-free connected and defect containing partially connected structures allows for analysis of the role of defects and grain boundaries on BCE transport properties. Because the state of the hydrated P2VP/NMP^+ I^- domains of fully microphase-separated BCE films are all equivalent at the same temperature and relative humidity, quantitative comparisons of conductivities and structure are possible between all of our samples with fully formed lamellae morphologies. σ_{BCE} of the BCE with a connected structure was 31-fold higher than σ_{BCE} of the BCE with a confined, partially connected morphology (2.2 versus 0.07 mS/cm). The lower σ_{BCE} observed in the partially connected BCE films could be fully accounted for by taking into account two structural differences between the samples: (1) the number of P2VP/NMP^+ I^- domains that are connected from one electrode to the other, and (2) the tortuosity (distance traveled between electrodes) of the connected domains.

The quantitative analysis was made using the equation

$$\sigma_{pc,eff} = \frac{m_{pc}}{m_c}\frac{l_c}{l_{pc}}\sigma_c \quad (4)$$

where $\sigma_{pc,eff}$ is the estimated effective conductivity of the partially connected morphology based on the assumptions above, σ_c is the conductivity of the connected morphology, m_{pc} is the total number of connected paths for the partially connected morphology, m_c is the total number of connected paths for the connected morphology, l_{pc} is the average length of the conduction path for the partially connected morphology, and l_c is the average length of the conduction path for the connected morphology.

The values of m_{pc}, m_c, l_{pc}, and l_c were determined by inspecting and performing image analysis on scanning electron micrographs of 1000 trenches in selected samples and counting and averaging the total number of connected pathways and the increase in the transport path length due to increased tortuosity. The statistics for the analysis are recorded in Figure 4. We determined m_c to be 27 650 connected paths by counting a total of 7 connected paths per trench and multiplying by 3950, which is the total number of trenches. Next, m_{pc} was determined by identifying and counting the connected paths in 1000 randomly selected trenches. Image analysis showed only 300 of 1000 trenches had connected pathways, and the vast majority of the 300 trenches contained only a single connected path. The trenches with zero connected paths were similar in morphology but every

DOI: 10.1021/acs.nanolett.9b01758
Nano Lett. XXXX, XXX, XXX−XXX

P2VP/NMP$^+$ I$^-$ channel was blocked by at least one PS domain barrier. The analysis of one trench shown in Figure 3d illustrates by example how we determined the number of pathways per trench if a connection existed. The number of connected pathways per trench was determined at the bottleneck where the ion transport would be gated. For example, the partially connected BCE structure analyzed in Figure 3d had seven separate ion conduction paths that make contact with the electrode. However, at the cross section with the smallest number of connected channels (i.e., the middle of the film), only a single channel is highlighted in blue. Therefore, this trench was determined to contain only one connected path out of seven. Additional examples of partially connected morphologies are shown in Figure 2d and the compiled count of trenches with specific number of connected domains is shown in Figure 4a. The m_{pc} value of 1185 was calculated by multiplying the fraction of connected trenches (300/1000) by the total number of trenches (3950) where each trench contained only one connected path. The conduction pathlengths l_{pc} and l_c were determined by tracing the shortest connected path from one electrode to the other on the SEM image and determining the length of the traced line using ImageJ graphic analysis software. The conduction pathways identified in the partially connected structure were more tortuous in comparison to the connected structure. The distribution of trenches with specific lengths of connected paths are shown in Figure 4b. Because of the higher tortuosity, the connected pathways in the partially connected morphology were measured to have an l_{pc} of 1.4 μm. l_c of the connected morphology is simply the separation distance of the electrodes in the IDE, namely 1 μm. Using the values of m_{pc}, m_c, l_{pc}, and l_c in eq 4 and testing the hypothesis that σ is proportional to the number of paths and inversely proportional to the path length, we estimate σ_{pc} to be 0.067 mS/cm, a value that compares very favorably with the experimentally determined value of 0.07 ± 0.05 mS/cm. The values are tabulated in Table 1. Using eq 4, the unconnected morphology would have an m value of 0, resulting in a calculated conductivity of zero. Note: conductance was used to compare the two morphologies instead of resistance because conductance scales with the total number of connected domains. The derivation of eq 4 is explained in the Supporting Information.

Table 1. Structure Parameters m and l Extracted from Structure Analysis of SEM Micrographs and the Calculated Conductivities Using Equation 4, m_c, l_c, and σ_c

	units	connected	partially connected	unconnected
m		27650	1185	0
l	μm	1	1.4	
σ	mS/cm	2.2	0.067	0

The C value from the equivalent circuit model can provide valuable structural information that is complementary to that derived from the conductivity analysis. Whereas the connected structure has very small differences in C from that of the homopolymer, the partially connected morphology has a C value that is higher by an order of magnitude. This suggests that substantial charge accumulation occurs in the defective structures of the partially connected films. Defect structures that exist in the partially connected domains include (1) dead ends of connected ion conduction paths (colorized yellow in Figure 3b) and (2) disconnected ion conduction pathways (colorized gray in Figure 3b). Furthermore, C value for the unconnected morphology with the highest number of disconnected domains was higher by an order of magnitude compared to the partially connected morphology. From this comparison, we can speculate that values of C derived from the EIS data are a measure of the relative volume fractions of material that are "dead" to transport due to defects and grain boundaries. In this sense, reporting the C value and looking for order of magnitude differences between homopolymer and nanostructured samples may be a useful tool to estimate the relative magnitude that structure and processing is playing in bulk measurements for which structure cannot be determined independently.

To further explore the properties of defect structures and to take a small step from the confined two-dimensional structures presented above toward more three-dimensional structures, (or at least unconfined two-dimensional structures), we also investigated BCE films with fingerprint lamella patterns on the IDEs without the confining HSQ guiding topography. The σ_{BCE} of the fingerprint structure was found to be a factor of 7 higher than the σ_{BCE} of the partially connected structure (0.5 versus 0.07 mS/cm), whereas C remained almost constant. The 7-fold increase in σ_{BCE} suggests that the fingerprint structure without the guiding topography provided more connected pathways between the electrodes, perhaps with longer more tortuous routes than were possible when confined by the HSQ guides. The σ_{BCE} of the fingerprint structure was also only an order of magnitude lower than σ_{HOMO} (0.5 versus 6 mS/cm), and this difference is expected to decrease further upon moving to a fully three-dimensional domain structure for which there are additional pathways to circumvent defects. The fact that the C value was equivalent between the two samples, and was much higher than C of the connected structure or homopolymer, suggests that despite more pathways there is still a significant fraction of the fingerprint films that did not contribute to the σ_{BCE}. An analogous observation has been reported by Diederichsen et al.[35] who studied electron transport in fingerprint BCP morphology templated gold nanowires. A discrete fraction of disconnected domains can reduce the conductivity by increasing tortuosity of connected paths and limiting the conductive volume.

In conclusion, the use of thin films and IDEs allowed for quantitative determination of structure property relationships in BCEs. Defects and grain boundaries often create dead ends for pathways of the conducting component with the net result of reduced conductivity as substantial volume fractions of material are no longer active in transport processes. The results of this study complement the past literature and improve our understanding of the use, potential caveats, and shortcomings of eq 1 and EMT to analyze transport in these materials. Whereas f is usually considered to account for structural information and has been used as a basis for comparison of differences in structure, in practice it is often better described as an empirical efficiency factor. Lumped into f is tortuosity, the impact of defects and grain boundaries, an effective volume fraction of conducting material, and perhaps even the possibility that the pure conducting material in the nanostructured confinement does not have the same conductivity of the pure conducting material in the bulk. Of these factors, only defects and grain boundaries can potentially reduce σ_{BCE} by an order of magnitude or more compared to the σ_{HOMO}; the reduction in conductivity due to tortuosity or an effective ϕ_{COND} is likely maximized at a factor of two or three. Finally,

DOI: 10.1021/acs.nanolett.9b01758
Nano Lett. XXXX, XXX, XXX−XXX

there is opportunity to combine thin film experiments and analysis as described here with bulk measurements on the same material; the complementary information may yield the fundamental understanding necessary for the design of materials and strategies for processing to realize selective and highly conducting membranes for electrochemical applications.

Materials. The block copolymer PS-*b*-P2VP (Mn of 25 kg mol^{-1} PS, 22 kg mol^{-1} P2VP) was received from Polymer Source and used as is. The monohydroxy terminated random copolymer brush (P(S-*r*-2VP)-OH) was synthesized as described in the Supporting Information. The neutral preference surface was formed using the P(S-*r*-2VP)-OH brush with 69% of the repeat units comprising of PS while the weakly preferential surface was formed using the P(S-*r*-2VP)-OH with 48% of the repeat units comprising of PS. All other chemicals (methyl iodide, toluene, *N*,*N*-dimethyformamide (DMF), methyl isobutyl ketone (MIBK), tetrahydrofuran (THF), acetone, and 2-propoanol (IPA)) were received from Sigma-Aldrich or Fisher Scientific and used without further purification. The gold interdigitated electrodes with HSQ guiding stripes were fabricated on semiconducting polished silicon wafers (1 μm thermally grown oxide layer) obtained from WRS materials. PMMA 950 k MW and MMA 6.5 photoresists were obtained from MicroChem Corporation and used as is for photolithography fabrication of the gold electrode layer. The HSQ photoresist FOX22 used for the guiding stripe layer was obtained from Du Pont Chemicals and diluted to 1:2 (v/v FOX22/MIBK) prior to use to control the thickness of the final film.

Fabrication of Interdigitated Electrodes with Nanoscale Trenches. Silicon wafers with a 1 μm thick, thermally grown oxide was cleaned with piranha solution (70:30 v/v mixture of concentrated sulfuric acid and 35 wt % hydrogen peroxide) for 30 min at 130 °C. The wafer was dehydrated on a hot plate at 80 °C for 15 min prior to being spun coat with a bilayer photoresist of MMA 6.5 (120 nm) and PMMA 950A (140 nm). The device pattern was written using the NFD JEOL JBX-9300FS electron beam lithography system with an acceleration voltage of 100 kV and a dose of 1200 $\mu C/cm_2$, and was developed with 1:3 v/v MIBK/IPA solution for 30 s, rinsed in IPA, and blown dry with N_2. The sample was then subject to 8 s of O_2 plasma to descum the lithographic features prior to evaporation of 10 nm of a titanium adhesion layer followed by a 90 nm gold layer using the AJA ATC-Orion electron beam evaporation chamber. The wafer was soaked in *N*-methyl-2-pyrrolidone at 80 °C for 15 min under subtle agitation for liftoff. The HSQ trench pattern was written using the NFD JEOL JBX-9300FS electron beam lithography system with an acceleration voltage of 100 kV and a dose of 1400 $\mu C/cm^2$ and was developed with CD26 for 3 min, rinsed in DI water, and blown dry with N_2. Alignment marks were used to orient the topographic features in HSQ relative to the interdigitated electrodes.

Control of Morphology in the Nanoscale Trenches. The substrate, HSQ features, and the gold electrodes were grafted or physiosorbed with hydroxyl-terminated (P(S-*r*-2VP)-OH) brushes. The brushes were deposited by spin coating a film of P(S-*r*-2VP)-OH (1 wt % dissolved in toluene), annealing at 200 °C for 2 h, rinsing away the excess by soaking in a toluene bath at 60 °C with periodic stirring by hand, rinsed in IPA, then blown dry with N_2.[27]

Characterization. Top-down SEM images of the self-assembled BCE films were taken with the Carl Zeiss−Merlin field emission scanning electron microscope. The acceleration voltage was 1.0 kV with a working distance of 3 to 4 mm using an in-lens detector. One nanometer of Pt/Pd was sputtered onto the surface of the device using the Cressington 108 Auto Sputter Coater to reduce electron beam charging and improve the image quality. Image processing of the lamellar structure was done via a visual Python analysis code explained in the Supporting Information and Figure S3. The electrochemical properties of the samples were probed using the Gamry reference 600 potentiostat ac EIS. EIS measurements were made from 1 MHz to 1 Hz[36−38] by connecting the IDEs to larger two-probe contact pads wired to the potentiostat/galvanostat. The measurements were made in a chamber with controlled temperature (25 °C) and relative humidity (95% RH) after an equilibration period of at least 24 h. Humidity-controlled testing at 25 °C and 95% RH eliminates undesired condensation of water at the interfaces but hydrates the P2VP/NMP^+ I^-) domains, enabling iodide transport at a common device operating condition.

■ ASSOCIATED CONTENT

Supporting Information

The Supporting Information is available free of charge on the ACS Publications website at DOI: 10.1021/acs.nanolett.9b01758.

IDE device design, the schematics of the solvent vapor annealing chamber, RH and temperature controlled electrochemical test setup, the quantified structure parameter analysis, additional connected trench images, raw electrochemical data, and extracted model fit values for the structures, synthesis of the monohydroxy terminated random copolymer brush (P(S-*r*-2VP)-OH), hydrated thickness calculations, justification of conductivity calculation for connected and partially connected structures, and the interpretation of the *C* data (PDF)

■ AUTHOR INFORMATION

Corresponding Author

*E-mail: nealey@uchicago.edu.

ORCID

Yu Kambe: 0000-0002-1422-350X

Christopher G. Arges: 0000-0003-1703-8323

Juan de Pablo: 0000-0002-3526-516X

Paul F. Nealey: 0000-0003-3889-142X

Notes

The authors declare no competing financial interest.

■ ACKNOWLEDGMENTS

This work was primarily supported by the U.S. Department of Energy, Basic Energy Sciences, Materials Sciences, and Engineering Division. Y.K. acknowledges support from the National Science Foundation Graduate Fellowship Program (NSF DGE-1144082). This research used resources available through the Center for Nanoscale Materials, a U.S. Department of Energy Office of Science user facility operated by Argonne National Laboratory under Contract No. DE-AC02-06CH11357, and the NSF MRSEC shared user facilities at the University of Chicago (NSF DMR-1420709).

DOI: 10.1021/acs.nanolett.9b01758
Nano Lett. XXXX, XXX, XXX−XXX

ABBREVIATIONS

BCP, block copolymer; BCE, block copolymer electrolytes; EMT, effective medium theory; SEM, scanning electron microscopy; IDE, interdigitated electrodes; HSQ, hydrogen silsesquioxane; RH, relative humidity; EIS, electrochemical impedance spectroscopy; MeI, methyl iodide

REFERENCES

(1) Elabd, Y. a.; Hickner, M. a. *Macromolecules* **2011**, *44*, 1−11.
(2) Parrondo, J.; Ramani, V. *J. Electrochem. Soc.* **2014**, *161* (10), F1015−F1020.
(3) Panday, A.; Mullin, S.; Gomez, E. D.; Wanakule, N.; Chen, V. L.; Hexemer, A.; Pople, J.; Balsara, N. P. *Macromolecules* **2009**, *42* (13), 4632−4637.
(4) Sun, J.; Stone, G. M.; Balsara, N. P.; Zuckermann, R. N. *Macromolecules* **2012**, *45*, 5151−5156.
(5) Doyle, R. P.; Chen, X.; Macrae, M.; Srungavarapu, A.; Smith, L. J.; Gopinadhan, M.; Osuji, C. O.; Granados-Focil, S. *Macromolecules* **2014**, *47* (10), 3401−3408.
(6) Hallinan, D. T.; Mullin, S. a.; Stone, G. M.; Balsara, N. P. *J. Electrochem. Soc.* **2013**, *160* (3), A464−A470.
(7) Trapa, P. E.; Huang, B.; Won, Y.-Y.; Sadoway, D. R.; Mayes, A. M. *Electrochem. Solid-State Lett.* **2002**, *5* (5), A85−A88.
(8) Ruzette, A.-V. G.; Soo, P. P.; Sadoway, D. R.; Mayes, A. M. *J. Electrochem. Soc.* **2001**, *148* (6), A537−A543.
(9) Singh, M.; Odusanya, O.; Wilmes, G. M.; Eitouni, H. B.; Gomez, E. D.; Patel, a J.; Chen, V. L.; Park, M. J.; Fragouli, P.; Iatrou, H.; Hadjichristidis, N.; Cookson, D.; Balsara, N. P. *Macromolecules* **2007**, *40* (13), 4578−4585.
(10) Buriez, O.; Han, Y. B.; Hou, J.; Kerr, J. B.; Qiao, J.; Sloop, S. E.; Tian, M.; Wang, S. *J. Power Sources* **2000**, *89* (2), 149−155.
(11) Wang, X.; Goswami, M.; Kumar, R.; Sumpter, B. G.; Mays, J. *Soft Matter* **2012**, *8* (11), 3036−3052.
(12) Young, W. S.; Epps, T. H. *Macromolecules* **2012**, *45* (11), 4689−4697.
(13) Chen, X. C.; Wong, D. T.; Yakovlev, S.; Beers, K. M.; Downing, K. H.; Balsara, N. P. *Nano Lett.* **2014**, *14* (7), 4058−4064.
(14) Majewski, P. W.; Gopinadhan, M.; Jang, W.-S. S.; Lutkenhaus, J. L.; Osuji, C. O. *J. Am. Chem. Soc.* **2010**, *132* (49), 17516−17522.
(15) Sax, J.; Ottino, J. M. *Polym. Eng. Sci.* **1983**, *23* (3), 165−176.
(16) Hallinan, D. T., Jr.; Balsara, N. P. *Annu. Rev. Mater. Res.* **2013**, *43* (1), 503−525.
(17) Irwin, M. T.; Hickey, R. J.; Xie, S.; So, S.; Bates, F. S.; Lodge, T. P. *Macromolecules* **2016**, *49*, 6928.
(18) Majewski, P. W.; Gopinadhan, M.; Osuji, C. O.; Majewski, P. W.; Gopinadhan, M.; Osuji, C. O. *Polymers (Basel).* **2019**, *11* (5), 887.
(19) Chintapalli, M.; Chen, X. C.; Thelen, J. L.; Teran, A. A.; Wang, X.; Garetz, B. A.; Balsara, N. P. *Macromolecules* **2014**, *47* (15), 5424−5431.
(20) Chintapalli, M.; Le, T. N. P.; Venkatesan, N. R.; Mackay, N. G.; Rojas, A. A.; Thelen, J. L.; Chen, X. C.; Devaux, D.; Balsara, N. P. *Macromolecules* **2016**, *49* (5), 1770−1780.
(21) Hoarfrost, M. L.; Segalman, R. A. *Macromolecules* **2011**, *44*, 5281−5288.
(22) Majewski, P. W.; Gopinadhan, M.; Osuji, C. O. *Soft Matter* **2013**, *9* (di), 7106.
(23) Kambe, Y.; Arges, C. G.; Patel, S. N.; Stoykovich, M. P.; Nealey, P. F. *ECS Interface* **2017**, *26*, 61.
(24) Chintapalli, M.; Higa, K.; Chen, X. C.; Srinivasan, V.; Balsara, N. P. *J. Polym. Sci., Part B: Polym. Phys.* **2017**, *55*, 266−274.
(25) Arges, C. G.; Kambe, Y.; Suh, H. S.; Ocola, L. E.; Nealey, P. F. *Chem. Mater.* **2016**, *28* (5), 1377−1389.
(26) Han, E.; Kang, H.; Liu, C. C.; Nealey, P. F.; Gopalan, P. *Adv. Mater.* **2010**, *22* (38), 4325−4329.
(27) Ji, S.; Liu, C.-C.; Son, J. G.; Gotrik, K.; Craig, G. S. W.; Gopalan, P.; Himpsel, F. J.; Char, K.; Nealey, P. F. *Macromolecules* **2008**, *41* (23), 9098−9103.
(28) Sharon, D.; Bennington, P.; Liu, C.; Kambe, Y.; Dong, B. X.; Burnett, V. F.; Dolejsi, M.; Grocke, G.; Patel, S. N.; Nealey, P. F. *J. Electrochem. Soc.* **2018**, *165* (16), H1028−H1039.
(29) Yadav, R.; Fedkiw, P. S. *J. Electrochem. Soc.* **2012**, *159* (3), B340−B346.
(30) Semenov, A. N. *Macromolecules* **1993**, *26*, 6617−6621.
(31) Pesko, D. M.; Webb, M. A.; Jung, Y.; Zheng, Q.; Miller, T. F.; Coates, G. W.; Balsara, N. P. *Macromolecules* **2016**, *49* (14), 5244−5255.
(32) Webb, M. A.; Jung, Y.; Pesko, D. M.; Savoie, B. M.; Yamamoto, U.; Coates, G. W.; Balsara, N. P.; Wang, Z. G.; Miller, T. F. *ACS Cent. Sci.* **2015**, *1* (4), 198−205.
(33) Segal-Peretz, T.; Ren, J.; Xiong, S.; Khaira, G.; Bowen, A.; Ocola, L. E.; Divan, R.; Doxastakis, M.; Ferrier, N. J.; de Pablo, J.; Nealey, P. F. *ACS Nano* **2017**, *11* (2), 1307−1319.
(34) Semenov, A. N. *Macromolecules* **1992**, *25* (19), 4967−4977.
(35) Diederichsen, K. M.; Brow, R. R.; Stoykovich, M. P. *ACS Nano* **2015**, *9* (3), 2465−2476.
(36) Scrosati, B.; Croce, F.; Persi, L.; Soc, J. E.; Scrosati, B.; Croce, F.; Persi, L. *J. Electrochem. Soc.* **2000**, *147* (5), 1718−1721.
(37) Orazem, M. E.; Tribollet, B.; Chang, B.-Y.; Park, S.-M. *Annu. Rev. Anal. Chem.* **2010**, *3* (1), 207−229.
(38) Paul, D. K.; McCreery, R.; Karan, K. *J. Electrochem. Soc.* **2014**, *161* (14), F1395−F1402.

DOI: 10.1021/acs.nanolett.9b01758
Nano Lett. XXXX, XXX, XXX−XXX